A&A 417, 181–188 (2004)
DOI: 10.1051/0004-6361:20040032

Astronomy & Astrophysics

XMM-Newton spectral and timing observations of the millisecond pulsar PSR J0218+4232

N. A. Webb, J.-F. Olive, and D. Barret

Centre d'Étude Spatiale des Rayonnements, CNRS/UPS, 9 avenue du Colonel Roche, 31028 Toulouse Cedex 04, France

Received 17 March 2003 / Accepted 18 November 2003

Abstract. We present *XMM-Newton* MOS imaging and PN timing data of the millisecond pulsar PSR J0218+4232. We confirm the previously detected pulsations of PSR J0218+4232 and we show that the folded lightcurve is dependent on energy. We present the broad band (0.2−10.0 keV) spectrum of this millisecond pulsar, as well as the spectra of: the pulsed emission, the individual pulses, the interpulse and the non-pulsed region and we compare our results with previous data from Rosat, BeppoSAX and Chandra. We discuss the results of the spectral fitting in the context of recent pulsar models.

Key words. X-rays: stars – stars: pulsars: individual: PSR J0218+4232 – radiation mechanisms: non-thermal – radiation mechanisms: thermal

1. Introduction

Pulsars show two different types of X-ray pulsations: soft pulsed emission with blackbody spectra where the emission is from the neutron star surface, such as cooling emission from the whole surface as a relic of the neutron star's birth and/or the emission from a heated region, most likely the polar cap; or pulsed emission with narrow pulses and hard power law spectra, where it is thought that the emission arises from the magnetosphere (see e.g. Saito et al. 1997; Kuiper et al. 1998; Takahashi et al. 2001, for further discussion). Therefore detecting not only a pulsation, but also determining the form of the pulse profile, could help to identify the underlying emission mechanism and detection of the polar cap thermal radiation would allow us to discriminate between various models of pulsars and study the properties of neutron star surface layers (Zavlin et al. 2002; Pavlov & Zavlin 1997; Zavlin & Pavlov 1998). Many millisecond pulsars (MSPs) such as PSR B1821–24 (e.g. Saito et al. 1997) and PSR B1937+21 (e.g. Takahashi et al. 2001), like many ordinary pulsars, show X-ray pulsations and have been observed to emit X-ray spectra that are well fitted by a hard power law. In contrast, it has been proposed that the millisecond pulsar PSR J0437–4715 emits thermal radiation from hot polar caps (Zavlin & Pavlov 1998; Zavlin et al. 2002).

The radio source J0218+4232 has been known for many years (Dwarakanath & Shankar 1990; Hales et al. 1993) although it was first confirmed to be a millisecond pulsar by Navarro et al. (1995), using radio observations made with the Lovell telescope in 1993. A pulse period of 2.3 ms was determined. Navarro et al. (1995) also showed that this luminous pulsar ($L_{400} > 2700$ mJy kpc^2 Navarro et al. 1995, where L_{400} is the luminosity at 400 MHz) is in orbit with a low mass white dwarf (0.2 $M_\odot$), with an orbital period of about two days. From the dispersion measure a lower limit on the distance of 5.7 kpc was derived.

Verbunt et al. (1996) showed evidence for PSR J0218+4232 at high energies, both in X-rays using ROSAT and γ-rays, using EGRET, the High-Energy Gamma-Ray Telescope aboard the Compton Gamma-Ray Observatory (CGRO). They also presented some indication of pulsation in both energy domains. Kuiper et al. (2000) provided stronger evidence for the detection of pulsed γ-ray emission from PSR J0218+4232, also using EGRET data. Kuiper et al. (1998) presented further evidence for X-ray pulsation at the radio pulse period using 98 ks of ROSAT data. They also likened the sharp pulses to those of PSR B1821–24 and the Crab pulsar, which indicates a magnetospheric origin of the pulsed X-ray emission. They also estimated that almost two thirds of the soft X-ray (0.1−2.4 keV) emission is non-pulsed, where Navarro et al. (1995) also stated that a large fraction of the radio emission is not pulsed. This lead them to the conclusion that PSR J0218+4232 is an aligned rotator. This was further supported by Stairs et al. (1999), using polarimetric radio observations.

BeppoSAX observations of PSR J0218+4232 (Mineo et al. 2000) provided detailed information on the pulsar's temporal and spectral emission properties (1.6−10 keV). They showed that pulse 1 (lying at $\phi = 0.8$, in Mineo et al. 2000) is much stronger than pulse 2 (lying at $\phi = 0.3$) in the 1.6−4 keV energy band, but that pulse 2 is much stronger than pulse 1 in the 4−10 keV energy band. Also at the higher energy no non-pulsed component was apparent above the background level. They determined a very hard power law fit, photon

Send offprint requests to: N. A. Webb,
e-mail: natalie.webb@cesr.fr

index = 0.61 ± 0.32, to the pulsed part of the spectrum, with a fixed column density of 5×10^{20} cm^{-2} (see Verbunt et al. 1996), which gave a flux of 4.1×10^{-13} ergs cm^{-2} s^{-1} (2−10 keV). The measured spectral indices of pulse 1 and pulse 2 were 0.84 ± 0.35 and 0.42 ± 0.36. The total spectrum was well fitted by a power law, with a photon index of 0.94 ± 0.22 and they found a flux of 4.3×10^{-13} ergs cm^{-2} s^{-1} (2−10 keV). Kuiper et al. (2002a) showed that the non-pulsed spectrum of PSR J0218+4232 has a softer spectrum than the pulsed emission, using 73 ks of Chandra data.

Recently, Kuiper et al. (2002a,b) presented multiwavelength (radio, X- and γ-ray) pulse profiles of PSR J0218+4232. They found that the two X- and γ-ray pulses are aligned and that the X-ray pulses are also aligned with two of the three radio pulses. This is a very interesting result as multiwavelength emission can help to discriminate between the different theoretical models proposed to describe the nature of millisecond pulsars, such as the polar cap models (see Harding & Muslimov 2002, and references therein) and the outer gap models (see Cheng et al. 2000, and references therein), and thus trace the origin of the emission. For example, in polar cap scenarios, γ-ray pulses should be accompanied by X-ray pulses at the same phase and with similar shapes (Rudak & Dyks 1999).

XMM-Newton combines the spectral capabilities of ROSAT (0.1−2.5 keV) and the BeppoSAX MECS (2−10 keV), which, when coupled with the *XMM-Newton*'s sensitivity, gives us unparalleled spectral information from low to high energies. We have thus used *XMM-Newton* to observe the millisecond pulsar PSR J0218+4232 to show the evolution of the pulsed profile from low energies (0.4−1.6 keV) to high energies (up to 12 keV). We present spectra of the pulsar as a whole and both the pulsed and non-pulsed components and we draw some conclusions about the nature of the emission from PSR J0218+4232.

2. Observations and data reduction

PSR J0218+4232 was observed by *XMM-Newton* on 2002 February 11−12. The observations spanned 37.2 ks (MOS cameras) and 36 ks (PN camera), but a soft proton flare affected 17 ks of the MOS exposure and 16.5 ks of the PN exposure. The MOS data were reduced using version 5.3.3 of the *XMM-Newton* SAS (Science Analysis Software). However, for the PN data we took advantage of the development track version of the SAS. Improvements have been made to the OAL (ODF (Observation Data File) access layer) task (version 3.106) to correct for spurious and wrong time values, premature increments, random jumps and blocks of frames stemming from different quadrants in the timing data in the PN auxiliary file, as well as correcting properly for the onboard delays (Kirsch et al. 2003). Using this version, our timing solution improved (see Sect. 3).

We employed the MOS cameras in the full frame mode, using a thin filter (see Turner et al. 2001). The MOS data were reduced using "emchain" with "embadpixfind" to detect the bad pixels. The event lists were filtered, so that 0−12 of the predefined patterns (single, double, triple, and quadruple pixel events) were retained and the high background periods were identified by defining a count rate threshold above the low background rate and the periods of higher background counts were then flagged in the event list. We also filtered in energy. We used the energy range 0.2−10.0 keV, as recommended in the document "EPIC Status of Calibration and Data Analysis" (Kirsch et al. 2002). The event lists from the two MOS cameras were merged, to increase the signal-to-noise.

The PN camera was also used with a thin filter, but in timing mode which has a timing resolution of 30 μs (Strüder et al. 2001). The PN data were reduced using the "epchain" of the SAS. Again the event lists were filtered, so that 0−4 of the predefined patterns (single and double events) were retained, as these have the best energy calibration and we filtered in energy. The document "EPIC Status of Calibration and Data Analysis" (Kirsch et al. 2002) recommends use of PN timing data above 0.5 keV, to avoid increased noise. We used, in general, the data between 0.6−12.0 keV as this had the best signal-to-noise, although we have also tried to exploit the data in the 0.4−0.6 keV band (see Sect. 3). The on-board event times expressed in the local satellite frame were subsequently converted to Barycentric Dynamical Time, using the SAS task "barycen" and the coordinates derived from 6.5 years of radio timing measurements, as given in Kuiper et al. (2002a).

3. Timing analysis

In the PN timing mode, all the two-dimensional spatial information is collapsed into a single dimension (x-direction). We extracted the pulsar data using a rectangular region centered on the pulsar.

We corrected the data for the orbital motion of the pulsar and the data were folded on the radio ephemeris given in Kuiper et al. (2002a). We verified that the corrections made to the timing data with the development version of the SAS are indeed correct. We tested frequencies at and around the expected frequency. We used a χ^2 test to determine the frequency at which the pulse profile was the strongest. We found the largest peak in the χ^2_ν versus change in frequency from the expected frequency at $\Delta\nu = 2 \times 10^{-6}$ s^{-1}, see Fig. 1. This is well inside the resolution of this dataset ($\sim 1/T_{\rm obs}$), which is 3×10^{-5} s^{-1}, thus we can conclude that the data reduction and analysis made to the dataset are reliable. The folded lightcurve (0.6−12 keV), data folded on the radio frequency, counts versus phase, is shown in Fig. 2. This lightcurve is very similar to the lightcurve presented by Kuiper et al. (2002a), where both pulses can be found at approximately the same phase (within the timing uncertainties of Chandra and *XMM-Newton* Kuiper et al. 2002a; Tennant et al. 2001; Kirsch et al. 2003). Fitting the two pulses with two Lorentzians and a background (in a similar way to Kuiper et al. 2002a), we find a pulse separation of $\phi = 0.491 \pm 0.022$ (90% confidence limit), consistent with previous results e.g. Kuiper et al. (1998, 2002a) and Mineo et al. (2000). The *FWHM* of the pulses are $\delta\phi_1 = 0.112 \pm 0.038$ for the pulse centred at phase $\phi_1 = 0.242 \pm 0.008$ and $\delta\phi_2 = 0.121 \pm 0.056$ for the pulse centred at $\phi_2 = 0.733 \pm 0.014$. These values are also consistent with the values presented in Kuiper et al. (2002a). Fitting the pulses with two Gaussians or fitting the pulses separately gives a similar result.

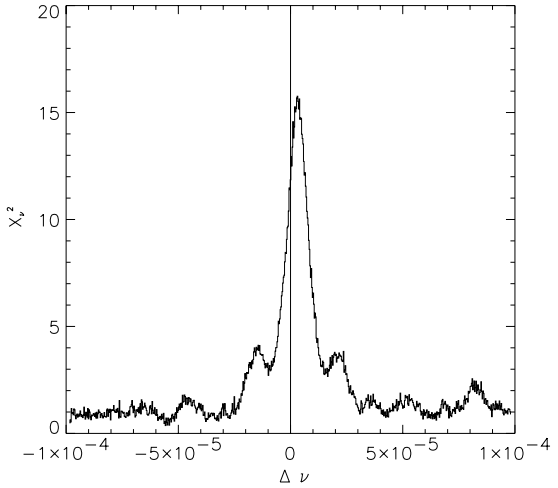

Fig. 1. χ^2_ν versus change in frequency from the expected pulsation frequency (shown as the solid vertical line at $\Delta\nu = 0.0$), calculated with the ephemeris of Kuiper et al. (2002a). See Sect. 3 for details.

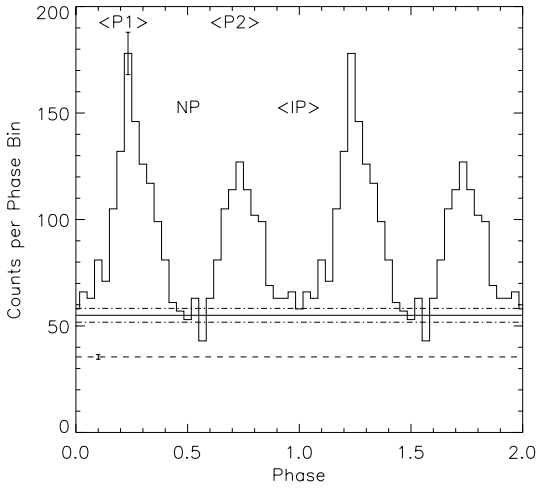

Fig. 2. Lightcurve folded on the ephemeris of Kuiper et al. (2002a) and binned into 30 bins, each of 77 μs. Two cycles are shown for clarity. Pulses 1 (P1) and 2 (P2) are indicated. Between these two pulses is the section defined as the non-pulsed region (NP). Between pulses 2 and 1 is the section defined as the interpulse (IP). A typical $\pm1\sigma$ error bar is shown. The dashed line shows the background level, where the error bar represents the $\pm1\sigma$ error. The solid line shows the DC level and the dashed-dotted lines represent the $\pm1\sigma$ error.

To calculate the DC (non-pulsed) level of our lightcurve we used the bootstrap method outlined by Swanepoel et al. (1996). The DC level is shown in Fig. 2 by the solid line and the two dashed-dotted lines show the $\pm1\sigma$ errors. The background level (also shown in Fig. 2, dashed line) was determined by extracting the data from a region in the same observation as the pulsar, centered 12 pixels (~50″) in the x-direction from the pulsar, where there were no other X-ray sources close to this position or in the full length of the y-direction. We verified that there were indeed no sources in this region, using the MOS imaging data (see Sect. 4). The extraction region chosen for the background was the same shape and size as the extraction region for the pulsar. We see evidence for both a DC interval between $\phi = 0.45-0.58$ (see Fig. 2) and an interpulse

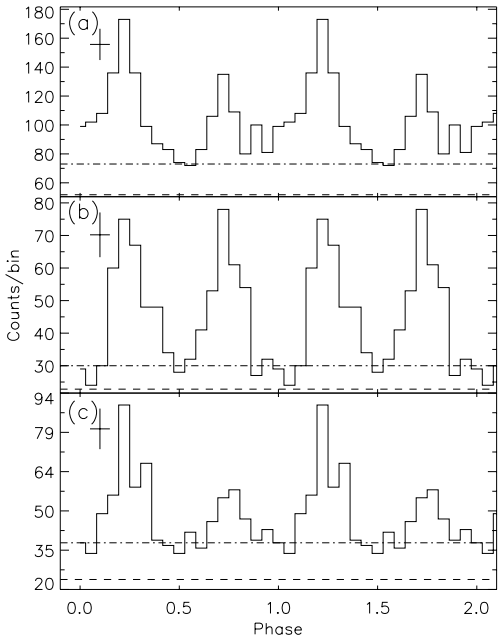

Fig. 3. Lightcurves folded on the pulse period and binned into 18 bins. **a)** 0.4−1.6 keV **b)** 1.6−4.0 keV **c)** 4.0−10.0 keV. Two cycles are shown for clarity. The dashed line indicates the background level, the dashed-dotted line indicates the DC level and an error bar represents the typical $\pm1\sigma$ error.

between $\phi = 0.88-1.11$, in similar places to those of Kuiper et al. (2002a), where the interpulse region has 10.5 ± 3.3 counts/bin more than the non-pulsed region. Thus we conclude that our X-ray pulse profile can be compared directly to the lightcurve of Kuiper et al. (2002a). We therefore refer to the pulse situated at $\phi_1 = 0.24$ as pulse 1 (phase = 0.11−0.45) and $\phi_2 = 0.73$ as pulse 2 (phase = 0.58−0.88) in the same way as Kuiper et al. (2002a). Subtracting the background from the total count distribution measured in the strip centred on the pulsar, we found a pulsed percentage of 69 ± 6% in the 0.6−12.0 keV band, similar to the value determined by Kuiper et al. (2002a), who found 64 ± 6% with Chandra in the 0.08−10.0 keV band. We find that pulse 1 contributes 65 ± 7% of the pulsed percentage and pulse 2 contributes 32±8%, where the ratio between the pulse 1 and the pulse 2 counts is 1.60±0.09 in the 0.6−12.0 keV band.

Given the large number of counts in our observations, we were also able to analyse the variations in the lightcurves as a function of energy. We chose the energy bands: 0.4−1.6 keV; 1.6−4.0 keV; and 4.0−10.0 keV, so that we could compare our results to those of Mineo et al. (2000), see Fig. 3. The data were folded as before and binned into 18 bins, where two cycles are presented for clarity.

The first thing that we notice from looking at Fig. 3 is that the lightcurves are remarkably different in the 3 energy bands, indicating that the spectra of the pulses are indeed quite dissimilar. Pulse 1 is always the strongest of the two pulses, but the ratio between the number of counts in the two pulses in the different energy bands varies quite dramatically. This can be seen quantitatively in Table 1. The softest and intermediate bands are consistent with the ratios found by Mineo et al. (2000). However Mineo et al. (2000) found that pulse 2 was

Table 1. Table showing the pulsed percentage and the ratio of pulse 1 to pulse 2 for the PSR J0218+4232 in different energy bands.

Energy band (keV)	Pulsed %	$\frac{\text{pulse1}}{\text{pulse2}}$
0.6−12.0	69 ± 6	1.60 ± 0.1
0.4−1.6	59 ± 7	2.1 ± 0.1
1.6−4.0	68 ± 11	1.1 ± 0.1
4.0−10.0	43 ± 12	2.5 ± 0.2

stronger than pulse 1 in the hardest band (0.4−10.0 keV), but they use a pulse width of $\phi = 0.37$ for pulse 2, whereas we use a pulse width of $\phi = 0.30$, which could account for the discrepancy. We also see evidence for the interpulse in the softest energy band.

As the ROSAT and BeppoSAX phasograms (Kuiper et al. 1998; Mineo et al. 2000) are not in absolute phase, it is important to determine which of the pulses correspond to our pulse 1 and 2. Kuiper et al. (2000) present the tentative alignment after cross-correlation of the two X-ray lightcurves (ROSAT HRI, 0.1−2.5 keV and BeppoSAX MECS 1.6−10.0 keV), where pulse 1 (the largest pulse in both the ROSAT and the BeppoSAX lightcurves) appears at approximately $\phi = 0.2$, as in our lightcurve and that of Kuiper et al. (2002a), which is in absolute phase. Thus we can compare pulses 1 and 2 in Mineo et al. (2000) with pulses 1 and 2 in this work.

Comparing our lightcurves with those presented in Mineo et al. (2000), we find a remarkable visual difference. In the intermediate energy band (1.6−4.0 keV), they find only one clear peak – pulse 1. However, we find that we have two pulses of similar strength. In the hardest band, we see that pulse 1 is strongest, in contrary to the BeppoSAX observations (Mineo et al. 2000). The discrepancies have yet to be explained, but they may be related, to some extent, to differences in the energy response of the different instruments. In the softest band (0.4−1.6 keV), we see that pulse 1 is strongest, similar to ROSAT (0.1−2.4 keV), (Kuiper et al. 1998; Mineo et al. 2000). Kuiper et al. (2002b) also find evidence that pulse 2 is stronger at higher energies than pulse 1, using RXTE data in the range 2−16 keV, as well as some evidence that pulse 2 is stronger than pulse 1 in the 2−8 keV range. Examining the 8−12 keV range, we find that pulse 2 is 1.5 times stronger than pulse 1. From this we have seen that the two pulses are spectrally quite dissimilar. With this in mind we investigated the pulse' spectra, as well as other regions of the lightcurve (see Sect. 5).

4. The MOS cameras' field of view

The sources in the MOS field of view were first detected using the SAS EPIC source detection task "eboxdetect", which employs a "local" source detection algorithm. A box of 5×5 pixels was used to detect point sources and then the same box was used on the background. To detect extended sources, two iterations were made with a box of 10 × 10 pixels and then 20 × 20 pixels, however only point sources were detected. A detection likelihood could then be calculated.

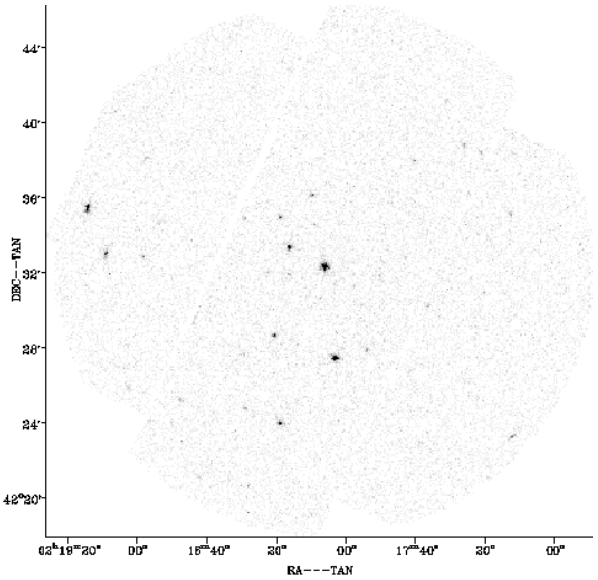

Fig. 4. MOS (20.5 ks) image of the pulsar field of view. The pulsar can be seen as the brightest source in the centre of the field of view.

42 sources have been detected using the SAS task "emldetect", using a maximum detection likelihood of 18 (approximately 4σ likelihood of detection) and ignoring those sources not found on both cameras (unless they lay outside the field of view or were in a chip gap). We calculate an unabsorbed flux limit of 1.0×10^{-14} ergs cm^{-2} s^{-1} (0.2−10.0 keV), using PIMMS (Mission Count Rate Simulator) Version 3.2, with a power law, photon index of 2 (as Hasinger et al. 2001). Kuiper et al. (2002a) found 51 sources in a comparable field of view. We detected 14 sources within the central 5′ radius (excluding the pulsar), where Mineo et al. (2000) found 7, using the ROSAT data of Kuiper et al. (1998). The whole field of view can be seen in Fig. 4.

5. Spectral analysis

The total energy spectrum of the MSP PSR J0218+4232 can be extracted from the MOS imaging data. However, as the lightcurves have been seen to vary dramatically from energy band to energy band (see Sect. 3), we have also used the PN timing data from which the phase resolved spectral information can be extracted, to isolate the spectra from different regions in the lightcurve. We have fitted these spectra with a variety of models, in an attempt to find which is the most appropriate.

5.1. MOS spectral analysis

We extracted the MOS spectra using an extraction radius of ∼1′ and rebinned the data into 15 eV bins. We used a similar neighbouring surface, free from X-ray sources to extract a background file. We used the SAS tasks "rmfgen" and "arfgen" to generate a "redistribution matrix file" and an "ancillary response file". We then used Xspec (Version 11.1.0) to fit the spectra. We binned up the data to contain at least 50 counts/bin. Fitting the MOS data together, we find that a good fit for the spectrum (between 0.2−10.0 keV) is a single absorbed power

law, photon index of 1.10 ± 0.06, χ^2_ν = 1.00 (29 degrees of freedom (d.o.f.)), when the $N_{\rm H}$ was frozen at 5×10^{20} cm^{-2}, see Verbunt et al. (1996). Allowing the $N_{\rm H}$ to vary, gives $N_{\rm H} = (7.6 \pm 4.3) \times 10^{20}$ cm^{-2} and a photon index of 1.19 ± 0.12, χ^2_ν = 1.04 (28 d.o.f.). A blackbody plus a power law also provides a good fit to the data (see Table 2, where the unabsorbed flux (ergs cm^{-2}s^{-1}) in the 0.6−10.0 keV range can also be found). A single blackbody gives a very poor fit to the data, $kT = 0.85 \pm 0.04$ keV, $\chi^2_\nu = 3.79$ (29 d.o.f.), when the $N_{\rm H}$ was frozen at 5×10^{20} cm^{-2}.

5.2. PN spectral analysis

5.2.1. The total pulsar spectrum

The PN spectra were extracted using regions as described in Sect. 3. We used the PN "timing and burst redistribution matrix file" supplied by the *XMM-Newton* Science Operations Centre[1]. Again we used Xspec to fit the spectra and we binned the data to have at least 50 counts/bin. The PN spectrum, between 0.6−10.0 keV, is well fitted by a single absorbed power law of photon index 1.08 ± 0.06 (see Fig. 5, left hand side), in good agreement with the MOS data (1.10 ± 0.06). The photon index of the power law fit is the same, within the errors, as that found by Mineo et al. (2000) (0.94 ± 0.22), who fitted the spectrum of PSR J0218+4232, observed by BeppoSAX, between 2−10 keV.

The advantage of the PN data is that we can fit the spectra from different regions in the lightcurve. In all the following fits, we assume $N_{\rm H} = 5 \times 10^{20}$ cm^{-2} and we simply subtracted a fraction of the background spectrum (as above) corresponding to the fraction of the pulsar phase interval that we were interested in, unless stated otherwise.

5.2.2. The pulsed region

We first extracted the spectrum of the whole of the pulsed region ($0.58 \leq \phi < 1.45$, see Fig. 2) and binned it up to have at least 30 counts/bin. The results of the best spectral fits and the unabsorbed flux of this pulse can be found in Table 2. We then subtracted the non-pulsed region from the pulsed region data, as Mineo et al. (2000), so that we could study the pulsed emission only. We find, that a power law gives a good fit to the data. The spectrum with the best power law fit, can be seen in Fig. 5, right hand side. However, we find that the power law photon index of the pulsed emission (1.19 ± 0.06) is softer than that found by Mineo et al. (2000) (0.61 ± 0.32), who fitted the BeppoSAX data between ∼2−10 keV, even taking into account the errors. The main difference between the *XMM-Newton* data and the BeppoSAX data is that *XMM-Newton* has spectral information down to ∼0.6 keV, whereas the BeppoSAX spectral information has a lower limit of about 2 keV. This discrepancy in the photon indices of the power law fits to the data sets may therefore stem from an excess of low energy photons in the *XMM-Newton* data, not observable by BeppoSAX.

[1] http://xmm.vilspa.esa.es/external/xmm_sw_cal/calib_frame.shtml

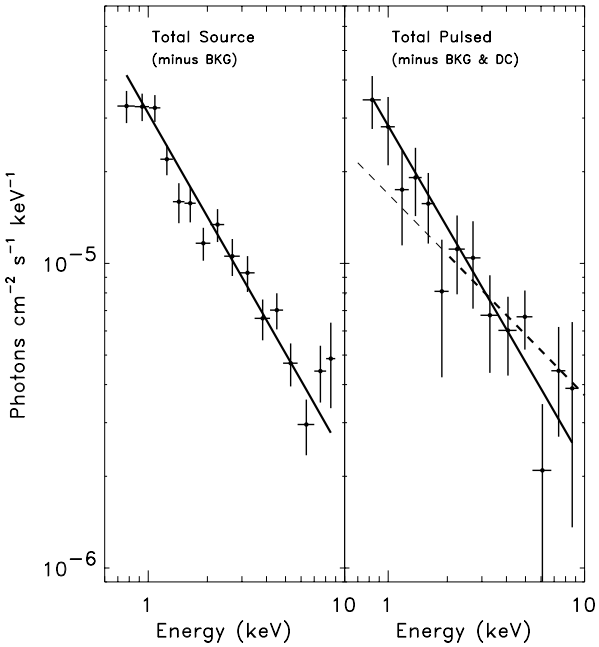

Fig. 5. The left hand plot shows the power law fit (solid line) to the unfolded total (pulsed + non-pulsed) pulsar spectrum using EPIC PN data. On the right hand side, the unfolded spectrum from the pulsed region only and the best fit to these data are shown. The thick dashed line is the best fit to the data above 2 keV, see Sect. 5.2.2, and the thin dashed line is the extrapolation of this fit, below 2 keV. Please note that the data have been rebinned to contain fewer bins than the data presented in Table 2, to make the plots clearer. The best fit is, however, the same as that presented in Table 2.

We therefore tried to fit our own data in the same energy band as Mineo et al. (2000). Using only this energy band we found that a power law, with a photon index of 0.68 ± 0.32 ($\chi^2_\nu = 0.99$, 15 d.o.f.), gave a good fit to the data. This power law fit can be seen as the thick dashed line in Fig. 5, right hand side. The photon index is consistent with the power law photon index found by Mineo et al. (2000). The thin dashed line indicates the extrapolation of this power law fit to lower energies. However, the data points at low energies (0.6−2 keV) deviate from the extrapolation of the power law fit. Including a blackbody model, where such thermal emission may be expected following theoretical work e.g. Zhang & Cheng (2003), gives an equally good fit to the data as a single power law fit. We also find that the power law photon index is now compatible with the photon index found by Mineo et al. (2000), with the BeppoSAX data. A two component blackbody model also gives a good fit to the data, see Table 2.

If we assume that the spectrum above 2 keV is best fitted by the power law given in Mineo et al. (2000) (as we have ruled out the single blackbody fit and also shown that we find a similar fit for our data above 2 keV), we can use this value to try to determine whether the single power law or a blackbody plus a power law gives the better fit to the data. Fitting the pulsed spectrum with the power law fixed at the Mineo et al. (2000) value, we find $\chi^2_\nu = 1.79$ (43 d.o.f.) and doing the same for the two component model, we find $\chi^2_\nu = 1.17$ (41 d.o.f.) (blackbody, $kT = 0.18 \pm 0.04$). Using an F-test we found that the

Table 2. Best fitting models to spectra from the MOS and PN data. In all the fits where no instrument is mentioned, the data is from the PN. Regions fitted are the whole lightcurve, the whole of the pulsed region, each of the pulses individually, the interpulse and the non-pulsed region ($N_{\rm H} = 5 \times 10^{20}$ cm^{-2}). The upper part of the table shows the data minus the background. The lower part of the table shows the data minus the non-pulsed region and the background. The flux given is unabsorbed flux (ergs cm^{-2} s^{-1}) in the 0.6−10.0 keV range, averaged over the whole of the pulse period, with errors of the order ±10%.

Region	Phase	Model	kT_1 (keV)	kT_2 (keV)	Photon index	χ^2_ν	d.o.f.	Flux ($\times 10^{-13}$)
All (MOS 1 & 2)	0.00–1.00	PL			1.10 ± 0.06	1.00	29	3.9
		BB + PL	0.29 ± 0.09		0.82 ± 0.22	0.96	27	
All (PN)	0.00–1.00	PL			1.08 ± 0.06	0.93	39	3.6
		BB + PL	0.19 ± 0.12		1.08 ± 0.14	0.99	37	
Pulsed	0.58–1.45	PL			1.19 ± 0.06	0.99	41	3.2
		2 BB	0.23 ± 0.19	1.12 ± 0.15		1.03	39	
Pulse 1	0.11–0.45	PL			1.20 ± 0.07	0.93	32	1.7
		BB + PL	0.29 ± 0.06		0.80 ± 0.24	0.85	30	
		2 BB	0.33 ± 0.03	1.83 ± 0.24		0.94	30	
Pulse 2	0.58–0.88	PL			1.15 ± 0.09	0.74	22	1.1
		2 BB	0.19 ± 0.05	1.04 ± 0.08		0.59	20	
Interpulse	0.88–1.11	PL			1.73 ± 0.33	0.79	6	0.4
		BB + PL	0.08 ± 0.05		1.34 ± 0.49	0.56	4	
Non-pulsed	0.45–0.58	PL			1.17 ± 0.37	0.55	5	0.2
		BB	0.68 ± 0.14			0.77	5	
Pulsed	0.58–1.45	PL			1.14 ± 0.13	0.99	41	2.7
		BB + PL	0.22 ± 0.10		0.82 ± 0.40	0.99	39	
		2 BB	0.25 ± 0.05	1.57 ± 0.31		0.89	39	
Pulse 1	0.11–0.45	PL			1.15 ± 0.13	1.13	32	1.5
		BB + PL	0.26 ± 0.07		0.55 ± 0.43	1.07	30	
		2 BB	0.29 ± 0.04	1.98 ± 0.53		1.04	30	
Pulse 2	0.58–0.88	PL			1.05 ± 0.20	0.87	22	0.8

PL = power law, BB = blackbody.

improvement in the fit was significant at the 3.8σ level. Even if we used the softest power law slope possible, taking into account the error on the Mineo et al. (2000) data, we found that the improvement in the fit was significant at the 2.6σ level. Thus we may have some indication that the two component model may be the best fit to the data.

5.2.3. Pulse 1

We then extracted the spectrum from pulse 1 only ($0.11 \leq \phi < 0.45$), binned it up to have at least 30 counts/bin and subtracted the background. The results of the best spectral fits and the unabsorbed flux of this pulse can be found in Table 2. Using the F-test we find that all the models that we have tried are equally probable as the most appropriate fit. The data from pulse 1 plotted with the best power law fit can be found in Fig. 6 (left hand side). A single blackbody and a thermal bremsstrahlung model give poor fits to the data. Subtracting the non-pulsed region from the pulse 1 data, as before, we find similar spectral fits to those found with the simple background extraction. The data plotted with the best power law fit can be seen in Fig. 6, right hand side. The power law spectral index that we find using the *XMM-Newton* data between 0.6−10.0 keV (1.15 ± 0.13) is larger than that found by Mineo et al. (2000) (2−10 keV), who found 0.84 ± 0.35, although it is compatible within the error bars. We did, however, try to fit our data above 2 keV, as in Sect. 5.2.2. We found that a harder power law with photon index 0.66 ± 0.29 gave a good fit to the data, $\chi^2_\nu = 1.29$ (19 d.o.f.). This is again compatible with the Mineo et al. (2000) result. The power law fit above 2 keV can be seen as the thick dashed line in Fig. 6, right hand side. The thin dashed line indicates the extrapolation of this power law fit to lower energies.

5.2.4. Pulse 2

Extracting the spectrum from pulse 2 only ($0.58 \leq \phi < 0.88$), binning it up to have at least 20 counts/bin and subtracting the background, we find the fits presented in Table 2. Again a single blackbody and a thermal bremsstrahlung model give poor fits to the data. The data plotted with the power law model can be found in Fig. 7 (left hand side). We subtracted the non-pulsed data from the pulse 2 data (as above). We again find similar results for the power law fit, as with the simple background extraction, however, as we found with the pulsed emission, the power law photon index is softer than that found by Mineo et al. (2000) (0.42 ± 0.36), again taking into account the errors. These data and the power law model can be found in Fig. 7 (right hand side).

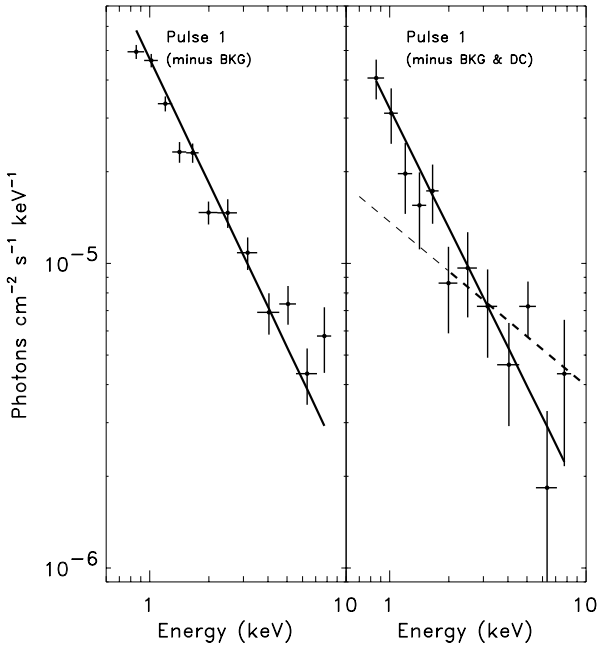

Fig. 6. Plots showing the power law fit (solid line) to pulse 1. On the left is pulse 1 minus the background contribution and on the right is pulse 1 minus the DC and background contributions. The thick dashed line is the best fit to the data above 2 keV, see Sect. 5.2.3, and the thin dashed line is the extrapolation of this fit to below 2 keV. These data are not averaged over the whole of the period, so the exposure time = $\Delta\phi \times T$ (where $\Delta\phi$ is the phase over which the pulse was extracted). Please note that the data have been rebinned to contain fewer bins than the data presented in Table 2, to make the plots clearer. The best fit is, however, the same as that presented in Table 2.

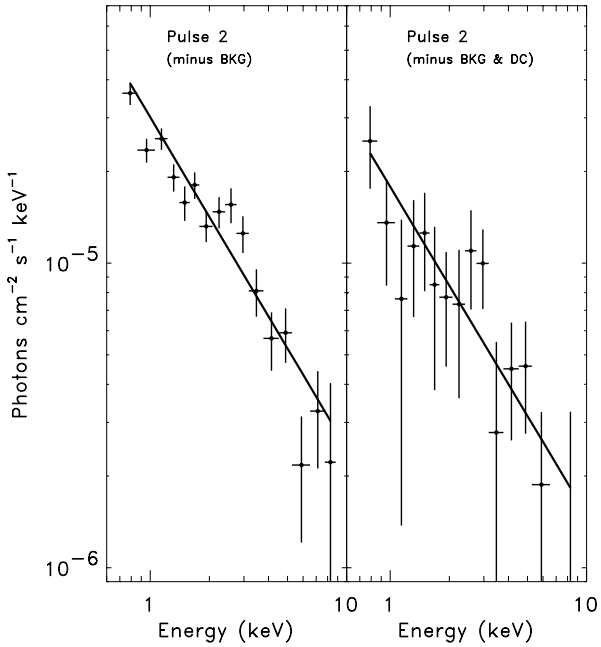

Fig. 7. Plots showing the best fit (power law, solid line) to pulse 2. On the left is pulse 2 minus the background contribution and on the right is pulse 2 minus the DC and background contributions. These data are not averaged over the whole of the period, so the exposure time = $\Delta\phi \times T$ (where $\Delta\phi$ is the phase over which the pulse was extracted). Please note that the data have been rebinned to contain fewer bins than the data presented in Table 2, to make the plots clearer. The best fit is, however, the same as that presented in Table 2.

5.2.5. The interpulse region

Fitting the spectrum to the interpulse region ($0.88 \leq \phi < 1.11$) in a similar way, we find the fits as given in Table 2. The errors are much larger in this case, due to the small number of bins. Again a single blackbody and a thermal bremsstrahlung model give poor fits to the data. We subtracted the non-pulsed data from the interpulse data (as above), however this resulted in too few counts to create a spectrum.

5.2.6. The non-pulsed region

Fitting the spectrum of the non-pulsed region ($0.45 \leq \phi < 0.58$) in a similar way (results in Table 2), we find that a simple power law gives the best fit to the data. In this case, a blackbody plus a power law model does not give a good fit. Taking the non-pulsed flux (0.6−10.0 keV) given in Table 2, and the total flux (0.6−10.0 keV) also given in Table 2, we find a pulsed fraction of 61^{+7}_{-5}%, consistent with the pulsed fraction given in Table 1 (0.6−12.0 keV).

6. Discussion

Thanks to the large collecting area of *XMM-Newton* (Jansen et al. 2001), even from a short observation of PSR J0218+4232, we are able to undertake detailed spectral analysis of the various components of the lightcurve.

PSR J0218+4232 shows a very hard spectrum and an analogy is often made between this MSP and two others, PSR B1821–24 and PSR B1937+21, which also show pulsed emission, large $\dot{E}$ values ($2{-}20\times10^{35}$ ergs s^{-1}) and X-ray spectra with photon indices less than 2 (Saito et al. 1997; Takahashi et al. 2001). These pulsars are in turn compared to the Crab pulsar, which shows narrow pulsations and a hard X-ray spectrum (Toor & Seward 1977). It is believed that such hard emission arises from the magnetosphere. However, the Crab pulsar shows pulses which have *FWHM* of ∼0.042 and 0.075 in phase at similar X-ray energies (Eikenberry & Fazio 1997), which are 2−3 times narrower than those of PSR J0218+4232. PSR B1821–24 also has a pulse width of less than 0.04 in phase (Rots et al. 1998; Saito et al. 1997) and those of PSR B1937+21 are also only ∼0.06 in phase (Takahashi et al. 2001). The larger width of the PSR J0218+4232 pulses may simply be due to it being an aligned rotator (Navarro et al. 1995). However, Luo et al. (2000) state that with their polar cap model, they can reproduce the wide double-peaked profile without assuming an aligned rotator. Nonetheless, the particularly hard spectrum, extending to γ-rays (Kuiper et al. 2000, 2002b) and the wider pulses shown by PSR J0218+4232 could indicate that it is a different kind of MSP to PSR B1821–24 and PSR B1937+21.

6.1. The pulsed emission

We have seen that the form of the pulsed emission varies significantly with energy (see Sect. 3 and Fig. 3). We have therefore

tried a variety of simple models to fit the pulsed emission data, see Sect. 5 and Table 2. For the pulsed spectrum and the spectra of pulses 1 and 2, we find that a single blackbody fit is not a good description of the data, but that a single power law does give a good fit. However, the photon indices that we find when fitting the *XMM-Newton* data, are significantly softer than those found by Mineo et al. (2000), when fitting the spectra observed with the BeppoSAX MECS between 2 and 10 keV. By fitting the *XMM-Newton* spectra with a two component model (blackbody plus power law, in the same way as for PSR J0437–4715 (Zavlin et al. 2002)) we recover the same power law photon indices found by Mineo et al. (2000), which could indicate that there may be additional emission below 2 keV and therefore not observable with BeppoSAX. Taking the blackbody temperature ($2.90 \pm 0.70 \times 10^6$ K) from the blackbody plus power law fit to pulse 1, we find a radius of emission of 0.37 ± 0.33 km (90% confidence limit), consistent with the temperature and radius of a polar cap (10^6–10^7 K and ~1 km e.g. Zhang & Cheng 2003; Zavlin & Pavlov 1998, and references therein).

There is some evidence from both the spectral fitting and the lightcurves presented in Sect. 3 that the interpulse region emits a softer spectrum than that of the two pulses (as also seen by Kuiper et al. 2002a).

6.2. The non-pulsed emission

With regards to the non-pulsed region, we find that a simple blackbody, with a temperature consistent with that determined using the ROSAT HRI, BeppoSAX MECS and Chandra instruments (Kuiper et al. 2002a), can fit the data. However, the radius of emission determined from this blackbody is only 0.10 ± 0.08 km. This indicates that from the small radius, the emission is unlikely to be from a polar cap. Kuiper et al. (2002a) suggest that this could nonetheless be thermal emission from the polar caps, if PSR J0218+4232 is a nearly aligned rotator and the viewing angle is small, so that the polar caps are always in sight. Alternatively, the data can be well described by a single power law, where the photon index is the same, within the errors, as is found to fit all the other sections of the lightcurve. This would be consistent with recent polar cap models, such as that of Zhang & Cheng (2003), where X-ray emission in these models consists of one power law and two thermal components. In these cases the nonthermal X-rays are produced by the synchrotron radiation of $e^{\pm}$ pairs created in a strong magnetic field near the stellar surface; the soft thermal X-rays are produced by heating of polar cap areas with a radius of the order of 1 km; and the medium hard thermal X-rays result from the polar cap heating by the return particles from the outer gap. This is consistent with data taken at higher energies (see Kuiper et al. 2000, 2002b), where Kuiper et al. (2000) determine that extrapolating a hard power law spectrum from the *XMM-Newton* spectral range is just in agreement with the OSSE upper limit.

7. Conclusions

We have presented *XMM-Newton* MOS imaging (0.2−10.0 keV) and PN timing (0.4−12.0 keV) data of PSR J0218+4232. Using the large number of counts, we have confirmed the previously detected pulsations of PSR J0218+4232 and we have shown that the form of the lightcurve varies with energy. We have shown that the broad band X-ray spectrum between 0.6−10.0 keV of the pulsed emission is softer than the spectrum measured between 2−10 keV by BeppoSAX, and we have shown some evidence that a simple power law may not be a good description of the 0.6−10.0 keV spectrum. A longer observation of this millisecond pulsar should establish whether or not this is indeed the case.

Acknowledgements. We would like to thank G. Ramsay, U. Lammers and M. Kirsch for their help in analysing the timing anomalies of the PN data and B. Gendre and P. Jean for their technical advice. We are also grateful to W. Kluźniak and J. Poutanen for several enlightening discussions.

References

Chen, K. S., Ruderman, M., & Zhang, L. 2000, ApJ, 537, 964
Dwarakanath, K. S., & Shankar, N. U. 1990, A&A, 11, 323
Eikenberry, S. S., & Fazio, G. G. 1997, ApJ, 476, 281
Hales, S. E. G., Baldwin, J. E., & Warner, P. J. 1993, MNRAS, 263, 25
Harding, A. K., & Muslimov, A. G. 2002, ApJ, 568, 862
Hasinger, G., Altieri, B., Arnaud, M., et al. 2001, A&A, 365, L45
Jansen, F., Lumb, D., Altieri, B., et al. 2001, A&A, 365, L1
Kirsch, M., & the EPIC Consortium 2002, XMM-SOC-CAL-TN-0018
Kirsch M.G.F., Becker W., Benlloch-Garcia S., et al., 2003, Proc. SPIE, 5165
Kuiper, L., Hermsen, W., Verbunt, F., & Belloni, T. 1998, A&A, 336, 545
Kuiper, L., Hermsen, W., Verbunt, F., et al. 2000, A&A, 359, 615
Kuiper, L., Hermsen, W., Verbunt, F., et al. 2002a, ApJ, 577, 917
Kuiper, L., & Hermsen, W. 2002b, The Gamma-Ray Universe, ed. A. Goldwurm, D. Neumann, & J. Tran Thanh Van (Vietnam: The Gioi Publishers)
Mineo, T., Cusumano, G., Kuiper, L., et al. 2000, A&A, 355, 1053
Luo, Q., Shibata, S., & Melrose, D. B. 2000, MNRAS, 318, 943
Navarro, J., de Bruyn, A. G., Frail, D. A., Kulkarni, S. R., & Lyne, A. G. 1995, ApJ, 455, L55
Pavlov, G. G., Shibanov, Y. A., & Zavlin, V. E. 1992, MNRAS, 253, 193
Pavlov, G. G., & Zavlin, V. E. 1997, ApJ, 490, 91
Rots, A. H., Jahoda, K., Macomb, D. J., et al. 1998, ApJ, 501, 749
Rudak, B., & Dyks, J. 1999, MNRAS, 303, 477
Saito, Y., Kawai, N., Kamae, T., et al. 1997, ApJ, 477, 37
Stairs, I. H., Thorsett, S. E., & Camilo, F. 1999, ApJS, 123, 627
Strüder, L., Briel, U., Dennerl, K., et al. 2001, A&A, 365, L18
Swanepoel, J. W. H., De Beer, C. F., & Loots, H. 1996, ApJ, 467, 261
Takahashi, M., Shibata, S., Torii, K., et al. 2001, ApJ, 554, 316
Tennant, A. F., Becker, W., Juda, M., et al. 2001, ApJ, 554, L173
Toor, A., & Seward, F. D. 1977, ApJ, 216, 560
Turner, M. J. L., Abbey, A., Arnaud, M., et al. 2001, A&A, 365, L27
Verbunt, F., Kuiper, L., Belloni, T., et al. 1996, A&A, 311, L9
Zavlin, V. E., Pavlov, G. G., & Shibanov, Y. A. 1996, A&A, 315, 141
Zavlin, V. E., & Pavlov, G. G. 1998, A&A, 329, 583
Zavlin, V. E., Pavlov, G. G., Sanwal, D., et al. 2002, ApJ, 569, 894
Zhang, L., & Cheng, K. S. 2003, A&A, 398, 639